Pekka Alitalo, Stanislav Maslovski, and Sergei Tretyakov. 2006. Three-dimensional isotropic perfect lens based on *LC*-loaded transmission lines. Journal of Applied Physics, volume 99, number 6, 064912.

© 2006 American Institute of Physics

Reprinted with permission.

Three-dimensional isotropic perfect lens based on *LC*-loaded transmission lines

Pekka Alitalo,[a] Stanislav Maslovski,[b] and Sergei Tretyakov[c]
Radio Laboratory/SMARAD, Helsinki University of Technology, P.O. Box 3000, FI-02015 TKK, Finland

(Received 22 September 2005; accepted 6 February 2006; published online 31 March 2006)

An isotropic three-dimensional flat lens of subwavelength resolution ("perfect lens"), based on the cubic meshes of interconnected transmission lines and bulk loads is proposed. The lens is formed by a slab of a loaded mesh placed between two similar unloaded meshes. The dispersion equations and the characteristic impedances of the eigenwaves in the meshes are derived analytically, with an emphasis on generality. This allows the designing of transmission-line meshes with desired dispersion properties. The required backward-wave mode of operation in the lens is realized with simple inductive and capacitive loads. An analytical expression for the transmission through the lens is derived and the amplification of evanescent waves is demonstrated. The factors that influence the enhancement of evanescent waves in the lens are studied and the corresponding design criteria are established. A possible realization of the structure is outlined. © *2006 American Institute of Physics*.
[DOI: 10.1063/1.2185840]

I. INTRODUCTION

In recent literature a lot of attention has been given to systems that are able to sense electromagnetic near fields (evanescent waves) and even to "amplify" them. The superlens proposed by Pendry[1] is one of such systems. His superlens is based on a Veselago medium[2] slab. The real parts of the permittivity and the permeability of the Veselago slab are both negative at certain wavelengths. Thus, the eigenwaves in the slab are *backward* waves, i.e., the wave phase and group velocities are antiparallel. This provides a negative refraction and focusing of waves in a planar slab, as was outlined by Veselago.[2] In addition, Pendry discovered that there was also a possibility to excite surface plasmon-polaritons on the slab surfaces and, due to that, amplify near fields.[1] The slab thickness can be of the order of the wavelength, so that the plasmon-polaritons excited at both sides of the slab are strongly coupled. Under certain conditions the plasmon-polariton excited at the back surface of the slab has a much stronger amplitude than that at the front surface. Such amplification of evanescent waves is the key principle in subwavelength imaging.

Known experimental realizations of volumetric artificial materials with negative parameters are highly anisotropic structures that utilize dense arrays of parallel thin conducting wires and variations of split-ring resonators.[3] The proposed isotropic arrangements use orthogonal sets of split rings[4] and also three-dimensional arrays of wires.[5] At the same time, there have been achievements in modeling of Veselago materials (and Pendry lens) with the help of *LC*-circuits or transmission-line (TL) based structures.[6–11] These networks do not rely on resonant response from particular inclusions, and the period of the mesh can be made very small as compared with the wavelength. These features allow realization of broadband and low-loss devices, which is extremely difficult if resonant inclusions are used.

The transmission-line network approach has been successfully realized in one- and two-dimensional networks, but up to now there have been doubts if it is possible to design a three-dimensional (3D) circuit analogy of the Veselago medium. The difficulties arise from the fact that such a 3D network requires a common ground connector. Any realization of such a ground will effectively work as a dense mesh of interconnected conductors that blocks the propagation of the electromagnetic waves practically the same way as a solid metal does (the structural period must be much less than the wavelength in order to realize an effectively uniform artificial material). In this paper we introduce isotropic three-dimensional transmission-line networks that overcome this difficulty.

In the TL-based networks that we study, the electromagnetic energy propagates through TL sections. The inside volume of every TL section is effectively screened from the other sections and from the outer space. This can be very naturally imagined with a 3D cubic-cell network of interconnected coaxial cable segments: the inner conductors of the segments are soldered at the network nodes; the same is done for the outer conductors. The whole system appears as a 3D pipe network where every pipe holds a central conductor and those conductors are crossing at the node points inside the pipes. A loaded TL network can be realized by placing loading elements inside the pipes. To couple the waves propagating inside the TL sections with free-space waves, one will have to use a kind of antenna array with every antenna feeding a particular TL segment. Waves in these transmission lines can be excited by incident fields of any polarization, depending on what kind of antennas couple external fields to the transmission lines. The properties of waves propagating inside the mesh structure do not depend on the way how the transmission lines are excited. If it is desirable to work with

[a]Electronic mail: pekka.alitalo@tkk.fi
[b]Electronic mail: stanislav.maslovski@tkk.fi
[c]Electronic mail: sergei.tretyakov@tkk.fi

 © 2006 American Institute of Physics

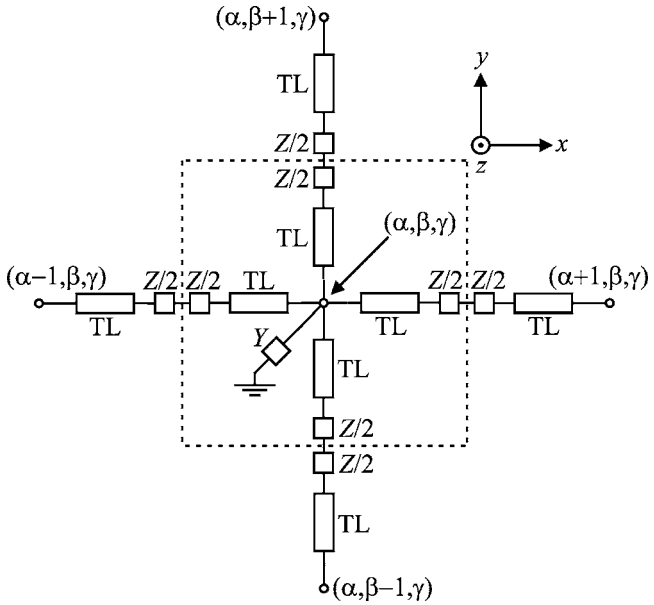

FIG. 1. Unit cell of a 3D backward-wave transmission-line network (enclosed by the dotted line). The transmission lines and impedances along the z axis are not shown. Transmission lines have the characteristic impedance $Z_{0,\mathrm{TL}}$ and length $d/2$ (d is the period of the structure).

arbitrary polarizations of the incident fields, one can use two similar superimposed 3D networks, each of them excited by antenna arrays of orthogonal polarizations.

When using transmission lines loaded with bulk elements we speak of waves in the meaning of discrete waves of voltages and currents defined at the loading positions. Let us note that in the TL sections *as such* the usual, forward waves propagate. Only because of the loading the discrete voltage and current waves appear as backward ones when appropriate loading impedances are used.

While completing this manuscript, we learned about another possible design of a 3D transmission-line analogy of a backward-wave material described in Ref. 12. That design is based on Kron's formal representation of Maxwell's equations as an equivalent electric circuit.[13] In Ref. 12 only one-dimensional (1D) propagation was studied analytically and 3D properties were analyzed numerically.

II. THREE-DIMENSIONAL TRANSMISSION-LINE NETWORKS

The proposed structure of 3D superresolution lens consists of two forward-wave (FW) regions and one backward-wave (BW) region. The 3D forward-wave networks can be realized with simple transmission lines and the 3D backward-wave network with inductively and capacitively loaded transmission lines. One unit cell of the BW network is shown in Fig. 1 (the unit cell is enclosed by the dotted line). In the 3D structure there are impedances $Z/2$ and transmission lines also along the z axis (not shown in Fig. 1). In view of potential generalizations, the loads are represented by series impedances $Z/2$ and shunt admittances Y, although for our particular purpose to realize a backward-wave network, the loads are simple capacitances and inductances. The equations that will be derived for these structures can be used for various implementations, but this paper will concentrate on the case when $Z=1/j\omega C$ and $Y=1/j\omega L$. The unit cell of the FW network is the same as in Fig. 1 but without the series impedances $Z/2$ and shunt admittance Y.

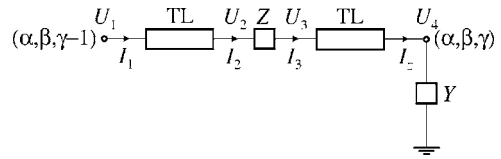

FIG. 2. Part of the 3D structure with transmission lines.

III. DISPERSION IN BACKWARD-WAVE AND FORWARD-WAVE NETWORKS

A. Dispersion equations

First, we will derive the dispersion relation for a simplified 3D BW network, i.e., we will not take into account the transmission lines. Such approximation is possible at low frequencies. Without the transmission-line segments, this derivation is quite simple and can be done by summing up all the currents that flow to the node (α,β,γ) and equating this sum with the current flowing to the ground (through admittance Y), see Fig. 1. The result is

$$\frac{1}{Z}(U_{\alpha+1,\beta,\gamma}+U_{\alpha,\beta+1,\gamma}+U_{\alpha,\beta,\gamma+1}+U_{\alpha-1,\beta,\gamma}+U_{\alpha,\beta-1,\gamma}+U_{\alpha,\beta,\gamma-1}-6U_{\alpha,\beta,\gamma})=U_{\alpha,\beta,\gamma}Y. \tag{1}$$

We look for a solution of the form $U_{\alpha,\beta,\gamma}=U_0e^{-j\mathbf{k}\cdot\mathbf{r}}$ ($\mathbf{r}=r_x\mathbf{x}_0+r_y\mathbf{y}_0+r_z\mathbf{z}_0$, $\mathbf{k}$ is wave vector), and if we use $q_x=k_xd$, $q_y=k_yd$ and $q_z=k_zd$, (1) can be reduced to

$$\frac{1}{Z}(e^{-jq_x}+e^{-jq_y}+e^{-jq_z}+e^{+jq_x}+e^{+jq_y}+e^{+jq_z}-6)=Y, \tag{2}$$

or

$$\cos(q_x)+\cos(q_y)+\cos(q_z)=\frac{ZY}{2}+3. \tag{3}$$

If we now insert $Z=1/j\omega C$ and $Y=1/j\omega L$, we get the dispersion relation for the LC-loaded network,

$$\cos(q_x)+\cos(q_y)+\cos(q_z)=-\frac{1}{2\omega^2LC}+3. \tag{4}$$

Next we want to take the transmission lines into account. The effect of the transmission lines can be derived by first evaluating a part of the three-dimensional network as the one shown in Fig. 2 and deriving the relation between the current that flows into a node and the voltages of adjacent nodes. If current I_1 is flowing towards node (α,β,γ) and the current that goes into node (α,β,γ) from the left is I_z, then using the ABCD-matrix for a transmission line we get

$$U_1=A_tU_2+B_tI_2, \tag{5}$$

$$I_1=C_tU_2+D_tI_2, \tag{6}$$

where

$$\begin{pmatrix} A_t & B_t \\ C_t & D_t \end{pmatrix} = \begin{bmatrix} \cos(k_{\mathrm{TL}}d/2) & jZ_{0,\mathrm{TL}}\sin(k_{\mathrm{TL}}d/2) \\ jZ_{0,\mathrm{TL}}^{-1}\sin(k_{\mathrm{TL}}d/2) & \cos(k_{\mathrm{TL}}d/2) \end{bmatrix}. \tag{7}$$

k_{TL} in (7) is the wavenumber of waves in the transmission lines. From (5) and (6) we can solve I_1 and I_2 as functions of U_1 and U_2:

$$I_1 = \frac{U_2(B_tC_t - A_tD_t) + D_tU_1}{B_t}, \tag{8}$$

$$I_2 = \frac{U_1 - A_tU_2}{B_t}. \tag{9}$$

Similarly for I_3 and I_z we get

$$I_3 = \frac{U_4(B_tC_t - A_tD_t) + D_tU_3}{B_t}, \tag{10}$$

$$I_z = \frac{U_3 - A_tU_4}{B_t}. \tag{11}$$

Next we can derive two equations for the current flowing through the series impedance Z and solve U_2 from both of them,

$$I_2 = Z^{-1}(U_2 - U_3) = \frac{U_1 - A_tU_2}{B_t}, \tag{12}$$

$$\Leftrightarrow U_2 = \frac{U_1 + Z^{-1}B_tU_3}{A_t + Z^{-1}B_t}; \tag{13}$$

$$I_3 = Z^{-1}(U_2 - U_3) = \frac{U_4(B_tC_t - D_tA_t) + D_tU_3}{B_t}, \tag{14}$$

$$\Leftrightarrow U_2 = \frac{U_4(B_tC_t - D_tA_t) + U_3(D_t + Z^{-1}B_t)}{Z^{-1}B_t}. \tag{15}$$

If we let U_2 in both equations be equal, we can solve U_3 as a function of U_1 and U_4,

$$U_3 = \frac{U_1Z^{-1}B_t - U_4(B_tC_t - D_tA_t)(A_t + Z^{-1}B_t)}{(D_t + Z^{-1}B_t)(A_t + Z^{-1}B_t) - Z^{-2}B_t^2}. \tag{16}$$

In order to derive an equation for I_z [the current that flows into node (α,β,γ) from the direction of node $(\alpha,\beta,\gamma-1)$] as a function of U_1 and U_4, we insert (16) into (11) and get

$$I_z = \frac{Z^{-1}B_tU_1 - (B_tC_t - D_tA_t)(A_t + Z^{-1}B_t)U_4}{[(D_t + Z^{-1}B_t)(A_t + Z^{-1}B_t) - Z^{-2}B_t^2]B_t} - \frac{A_t}{B_t}U_4. \tag{17}$$

If we use $U_1 = U_{\alpha,\beta,\gamma-1}$ and $U_4 = U_{\alpha,\beta,\gamma}$, then $I_z = S_{\mathrm{BW}}U_{\alpha,\beta,\gamma-1} + K_{\mathrm{BW}}U_{\alpha,\beta,\gamma}$. Because of the symmetry we can derive the dispersion relation exactly the same way as (1)–(4), and for the case $Z = 1/j\omega C$, $Y = 1/j\omega L$ the result is

$$\cos(q_x) + \cos(q_y) + \cos(q_z) = \frac{1}{2j\omega LS_{\mathrm{BW}}} - 3\frac{K_{\mathrm{BW}}}{S_{\mathrm{BW}}}, \tag{18}$$

where

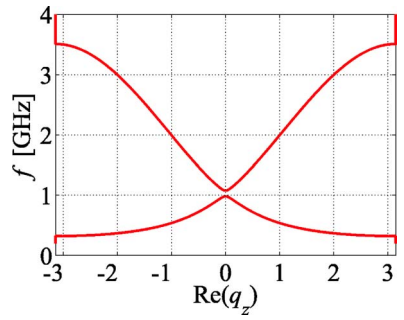

FIG. 3. (Color online) Dispersion curve for the backward-wave network. $C=5$ pF, $L=10$ nH, $d=0.012$ m, $\varepsilon_r=2.33$, and $Z_{0,\mathrm{TL}}=85\ \Omega$.

$$S_{\mathrm{BW}} = \frac{j\omega C}{(D_t + j\omega CB_t)(A_t + j\omega CB_t) + \omega^2C^2B_t^2}, \tag{19}$$

$$K_{\mathrm{BW}} = \frac{-(B_tC_t - D_tA_t)(A_t + j\omega CB_t)}{[(D_t + j\omega CB_t)(A_t + j\omega CB_t) + \omega^2C^2B_t^2]B_t} - \frac{A_t}{B_t}. \tag{20}$$

To derive the dispersion relation for the forward-wave network, we can use the equations derived for the backward-wave network letting $C \to \infty$ and $L \to \infty$. This way we get from (19) and (20) the following equations for S_{FW} and K_{FW}:

$$S_{\mathrm{FW}} = \frac{1}{B_t(A_t + D_t)}, \tag{21}$$

$$K_{\mathrm{FW}} = -\frac{B_tC_t - D_tA_t}{A_t + D_t}\frac{1}{B_t} - \frac{A_t}{B_t}. \tag{22}$$

From (18) we get the dispersion relation,

$$\cos(q_x) + \cos(q_y) + \cos(q_z) = -3\frac{K_{\mathrm{FW}}}{S_{\mathrm{FW}}}. \tag{23}$$

B. Typical dispersion curves

Dispersion curves for backward-wave and forward-wave networks can be plotted if the values of the transmission-line parameters and L and C are fixed. Let us choose the parameters of the TLs and the lumped components as: $L=10$ nH, $C=5$ pF, and $d=0.012$ m (the period of the network), $Z_{0,\mathrm{TL,BW}}=85\ \Omega$, $Z_{0,\mathrm{TL,FW}}=85\ \Omega$ (characteristic impedances of the TLs) and $\varepsilon_r=2.33$. See Figs. 3 and 4 for the examples

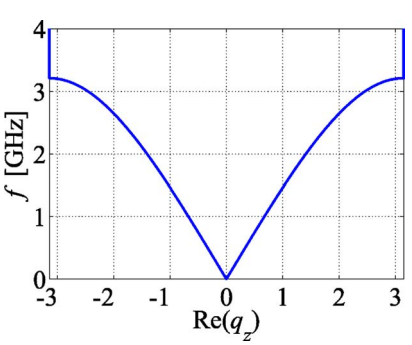

FIG. 4. (Color online) Dispersion curve for the forward-wave network. $d=0.012$ m, $\varepsilon_r=2.33$, and $Z_{0,\mathrm{TL}}=85\ \Omega$.

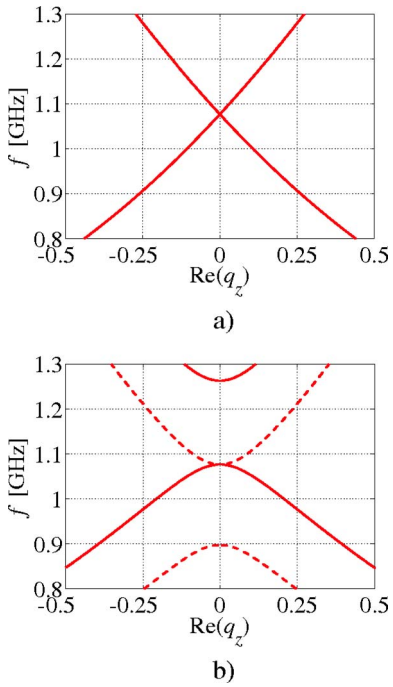

FIG. 5. (Color online) Dispersion curves for the backward-wave network. $L=10$ nH, $d=0.012$ m, $\varepsilon_r=2.33$, and $Z_{0,\mathrm{TL}}=85\ \Omega$. (a) $C=4.151$ pF. (b) Solid line: $C=3$ pF and dashed line: $C=6$ pF.

of dispersion curves when a z-directed plane wave is considered (i.e., $q_x=q_y=0$). $k_{\mathrm{TL}}=\omega\sqrt{\varepsilon_r}/c$, where c is the speed of light in vacuum. Notice that the BW network supports backward waves in the first passband ($0.32\ \mathrm{GHz}\leqslant f \leqslant 0.98\ \mathrm{GHz}$). In the second passband ($1.08\ \mathrm{GHz}\leqslant f \leqslant 3.50\ \mathrm{GHz}$), the BW network works as a normal FW network.

By tuning the capacitance C (or inductance L), the stopband between the BW and FW regions shown in Fig. 3 can be closed, see Fig. 5(a), where $C=C_0=4.151$ pF. As can be seen from Fig. 5(b), by changing the value of C from this "balanced" case, the stopband is formed either by moving the edge of the FW region up ($C<C_0$) or by moving the edge of the BW region down ($C>C_0$).

IV. THE CHARACTERISTIC IMPEDANCES OF BACKWARD-WAVE AND FORWARD-WAVE NETWORKS

Next the characteristic impedance of the backward-wave network is derived. If we assume that the interface between the FW and BW networks is at the center of capacitor C (see Fig. 2, where $Z=1/j\omega C$), then we can define the characteristic impedance at that point as

$$Z_{0,\mathrm{BW}}=\frac{U_2+U_3}{2I_2}=\frac{U_2+U_3}{2I_3}. \tag{24}$$

First, we have to express U_2, U_3, and I_3 (or optionally I_2) as functions of U_1 and U_4. We can use Eqs. (14)–(16). If we insert (16) into (15) and (14), we find U_2, U_3, and I_3 as functions of U_1 and U_4. Therefore we can present U_2, U_3, and I_3 simply as: $U_2=a_{\mathrm{BW}}U_1+b_{\mathrm{BW}}U_4$, $U_3=c_{\mathrm{BW}}U_1+d_{\mathrm{BW}}U_4$, and $I_3=e_{\mathrm{BW}}U_1+f_{\mathrm{BW}}U_4$.

Because $U_4=e^{-jq_z}U_1$ for a wave moving along the $+z$ direction, the characteristic impedance can be expressed as

$$Z_{0,\mathrm{BW}}=\frac{U_2+U_3}{2I_3}=\frac{a_{\mathrm{BW}}+b_{\mathrm{BW}}e^{-jq_z}+c_{\mathrm{BW}}+d_{\mathrm{BW}}e^{-jq_z}}{2e_{\mathrm{BW}}+2f_{\mathrm{BW}}e^{-jq_z}}, \tag{25}$$

where

$$a_{\mathrm{BW}}=\frac{D_t+j\omega CB_t}{(D_t+j\omega CB_t)(A_t+j\omega CB_t)+\omega^2C^2B_t^2}, \tag{26}$$

$$b_{\mathrm{BW}}=\frac{B_tC_t-D_tA_t}{j\omega CB_t}-\frac{D_t+j\omega CB_t}{j\omega CB_t}\frac{(B_tC_t-D_tA_t)(A_t+j\omega CB_t)}{(D_t+j\omega CB_t)(A_t+j\omega CB_t)+\omega^2C^2B_t^2}, \tag{27}$$

$$c_{\mathrm{BW}}=\frac{j\omega CB_t}{(D_t+j\omega CB_t)(A_t+j\omega CB_t)+\omega^2C^2B_t^2}, \tag{28}$$

$$d_{\mathrm{BW}}=-\frac{(B_tC_t-D_tA_t)(A_t+j\omega CB_t)}{(D_t+j\omega CB_t)(A_t+j\omega CB_t)+\omega^2C^2B_t^2}, \tag{29}$$

$$e_{\mathrm{BW}}=\frac{D_t}{B_t}\frac{j\omega CB_t}{(D_t+j\omega CB_t)(A_t+j\omega CB_t)+\omega^2C^2B_t^2}, \tag{30}$$

$$f_{\mathrm{BW}}=\frac{B_tC_t-D_tA_t}{B_t}-\frac{D_t}{B_t}\frac{(B_tC_t-D_tA_t)(A_t+j\omega CB_t)}{(D_t+j\omega CB_t)(A_t+j\omega CB_t)+\omega^2C^2B_t^2}. \tag{31}$$

To derive the characteristic impedance of the forward-wave network, we can use the equations derived for the backward-wave network if we insert $C\rightarrow\infty$ in them. If this condition applies, we get from (25)–(31),

$$Z_{0,\mathrm{FW}}=\frac{U_2+U_3}{2I_3}=\frac{a_{\mathrm{FW}}+b_{\mathrm{FW}}e^{-jq_z}+c_{\mathrm{FW}}+d_{\mathrm{FW}}e^{-jq_z}}{2e_{\mathrm{FW}}+2f_{\mathrm{FW}}e^{-jq_z}}, \tag{32}$$

where

$$a_{\mathrm{FW}}=c_{\mathrm{FW}}=\frac{1}{A_t+D_t}, \tag{33}$$

$$b_{\mathrm{FW}}=d_{\mathrm{FW}}=-\frac{B_tC_t-D_tA_t}{A_t+D_t}, \tag{34}$$

$$e_{\mathrm{FW}}=\frac{D_t}{B_t}\frac{1}{A_t+D_t}, \tag{35}$$

$$f_{\mathrm{FW}}=\frac{B_tC_t-D_tA_t}{B_t}-\frac{D_t}{B_t}\frac{B_tC_t-D_tA_t}{A_t+D_t}. \tag{36}$$

$Z_{0,\mathrm{BW}}$ and $Z_{0,\mathrm{FW}}$ can be plotted (25) and (32) as functions of the frequency if the transmission-line parameters and L and C are fixed. Let us choose the parameters of the TLs and

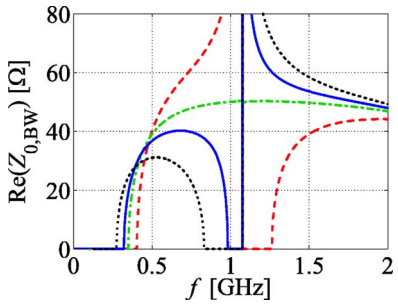

FIG. 6. (Color online) Characteristic impedance as a function of frequency for the backward-wave network. $L=10$ nH, $d=0.012$ m, $\varepsilon_r=2.33$, and $Z_{0,\mathrm{TL}}=85\ \Omega$. Dashed line: $C=3$ pF, dash-dotted line: $C=4.151$ pF, solid line: $C=5$ pF, and dotted line: $C=7$ pF.

the lumped components as: $C=5$ pF, $L=10$ nH, $d=0.012$ m, $\varepsilon_r=2.33$, $Z_{0,\mathrm{TL,BW}}=85\ \Omega$, and $Z_{0,\mathrm{TL,FW}}=70\ \Omega$. See Figs. 6 and 7 for examples of the characteristic impedances when a z-directed plane wave is considered (i.e., $q_x=q_y=0$). The effect of changing C on the characteristic impedance can be seen in Fig. 6, and the effect of changing $Z_{0,\mathrm{TL,FW}}$ on the characteristic impedance is shown in Fig. 7. Notice that for the BW network the characteristic impedance is continuous only in the "balanced" case ($C=4.151$ pF here), because in the stopbands the real part of the impedance is zero.

V. MATCHING OF FORWARD-WAVE AND BACKWARD-WAVE NETWORKS

We consider a lens with the axis parallel to the z axis. To have perfect imaging, the lens should support all spatial harmonics (i.e., waves with all possible transverse wave numbers k_t) of the source field and for those values of k_t, the longitudinal wave numbers $k_{z,\mathrm{FW}}$ and $k_{z,\mathrm{BW}}$ should be equal in magnitude but opposite in sign.

From Fig. 8 we can conclude that the matching of $|k_{z,\mathrm{FW}}|$ and $|k_{z,\mathrm{BW}}|$ (which corresponds to the relative refraction index of -1) can be achieved only at one frequency (depending on the parameters of the forward-wave and backward-wave networks). In Fig. 8 this frequency is $f=0.7279$ GHz. At this frequency the dispersion curves of the forward-wave and backward-wave networks intersect. In the analytical form this means that

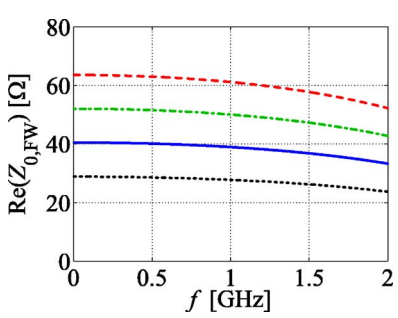

FIG. 7. (Color online) Characteristic impedance as a function of frequency for the forward-wave network. $d=0.012$ m, $\varepsilon_r=2.33$. Dotted line: $Z_{0,\mathrm{TL}}=50\ \Omega$, solid line: $Z_{0,\mathrm{TL}}=70\ \Omega$, dash-dotted line: $Z_{0,\mathrm{TL}}=90\ \Omega$, and dashed line: $Z_{0,\mathrm{TL}}=110\ \Omega$.

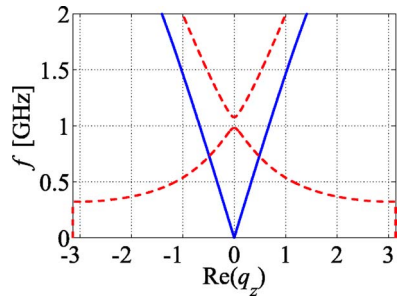

FIG. 8. (Color online) Dispersion curves for the forward-wave (solid line) and backward-wave (dashed line) networks. $C=5$ pF, $L=10$ nH, $d=0.012$ m, $\varepsilon_r=2.33$, $Z_{0,\mathrm{TL,BW}}=85\ \Omega$, and $Z_{0,\mathrm{TL,FW}}=70\ \Omega$. The transverse wavenumber $k_t=0$.

$$\frac{1}{2j\omega_0 L S_{\mathrm{BW}}(\omega_0)} - 3\frac{K_{\mathrm{BW}}(\omega_0)}{S_{\mathrm{BW}}(\omega_0)} = -3\frac{K_{\mathrm{FW}}(\omega_0)}{S_{\mathrm{FW}}(\omega_0)}, \tag{37}$$

as can be seen from (18) and (23). The dispersion curves in Fig. 8 are plotted so that q_x and q_y are zero (a plane wave moving along the z axis). From Fig. 8 it is seen also that for $f=0.7279$ GHz $|q_{z,\mathrm{BW}}|=|q_{z,\mathrm{FW}}|=0.4869$ when $k_t=0$. This means that the absolute value of the maximum wave number for propagating waves is approximately 40.6 m^{-1}.

In addition to matching the wave numbers (refractive indices), to realize an ideal "perfect lens" the interfaces between the forward-wave and backward-wave networks should also be impedance matched. If the two regions would not be matched, reflections from the interface would distort the field patterns both inside and outside the lens. As can be seen from Figs. 6 and 7, the characteristic impedances of the backward-wave network and the forward-wave network are about 40 Ω at the frequency where the wave numbers are matched (and when $C=5$ pF and $Z_{0,\mathrm{TL,FW}}=70\ \Omega$). Notice that the impedances of the transmission lines in the forward-wave network have been lowered from 85 to 70 Ω to achieve impedance matching of the forward-wave and backward-wave networks.

Next the effect of nonzero k_t on the matching is considered (at the optimal frequency). The minimum and maximum values of k_t can be found from $k_{t,\min}=-\pi/d$ and $k_{t,\max}=\pi/d$. From (18) and (23) we can plot $k_{z,\mathrm{BW}}$ and $k_{z,\mathrm{FW}}$ as functions of the transverse wave number ($k_t=\sqrt{k_x^2+k_y^2}$) if we fix the frequency. Now $k_{z,\mathrm{BW}}$ and $k_{z,\mathrm{FW}}$ are surfaces with variables k_x and k_y. By comparing these surfaces, it was seen that they were practically the same for all possible values of k_t. This happens only at the frequency $f=0.7279$ GHz, where the dispersion curves of the forward-wave and backward-wave networks intersect.

Because the characteristic impedances are functions of the ABCD matrices and k_z (and k_z is a function of k_t), we can plot $Z_{0,\mathrm{FW}}$ and $Z_{0,\mathrm{BW}}$ as functions of k_t if we fix the frequency. Now $Z_{0,\mathrm{BW}}$ and $Z_{0,\mathrm{FW}}$ are surfaces with variables k_x and k_y. By comparing these surfaces, it was seen that they were almost the same (less than one percent difference) for all possible values of k_t at $f=0.7279$ GHz. See Fig. 9 for a two-dimensional (2D) cut of the relative difference between

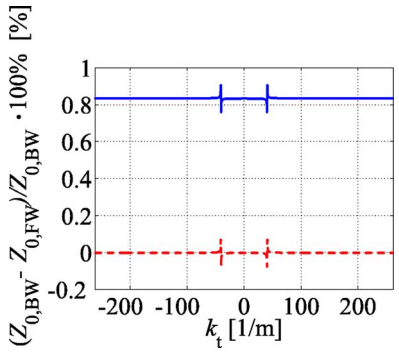

FIG. 9. (Color online) Relative difference $(Z_{0,\mathrm{BW}}-Z_{0,\mathrm{FW}})/Z_{0,\mathrm{BW}}$ as a function of k_t. $C=5$ pF, $L=10$ nH, $d=0.012$ m, $\varepsilon_r=2.33$, and $Z_{0,\mathrm{TL,BW}}=85\ \Omega$. Solid line: $Z_{0,\mathrm{TL,FW}}=70\ \Omega$, dashed line: $Z_{0,\mathrm{TL,FW}}=70.59\ \Omega$. $k_x=k_t$.

such surfaces (now $k_y=0$ and therefore $k_t=k_x$). The ideal perfect lens situation is achieved with $Z_{0,\mathrm{TL,FW}}=70.59\ \Omega$, as can be also seen from Fig. 9.

When the frequency deviates from the optimal value [for which (37) is true], the wave numbers and characteristic impedances are no longer matched. The effect of this is a distortion of the image seen in the image plane of the lens.

VI. TRANSMISSION OF THE SOURCE FIELD THROUGH THE LENS

The transmission coefficient of the lens can be solved by considering the incident and reflected fields in the lens system. Let us assume that the incident field outside the lens has the unit amplitude, the reflected field outside the lens has amplitude R, the incident field inside the lens has amplitude $Ae^{-jk_{z,\mathrm{BW}}z}$, and the reflected field inside the lens has amplitude $Be^{+jk_{z,\mathrm{BW}}z}$ (z is the distance from the front edge of the lens). From these values we can form the following equations (the length of the BW slab is l and the transmission coefficient of the BW slab is T_{Lens}, see Fig. 10):

$$1+R=A+B, \tag{38}$$

$$\frac{1-R}{Z_{0,\mathrm{FW}}}=\frac{A-B}{Z_{0,\mathrm{BW}}}, \tag{39}$$

$$T_{\mathrm{Lens}}=Ae^{-jk_{z,\mathrm{BW}}l}+Be^{+jk_{z,\mathrm{BW}}l} \tag{40}$$

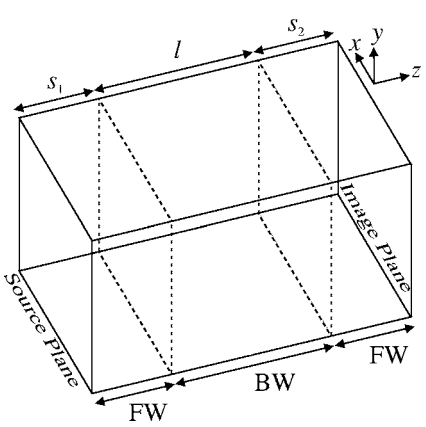

FIG. 10. A 3D "perfect lens" with distances l, s_1, and s_2 shown.

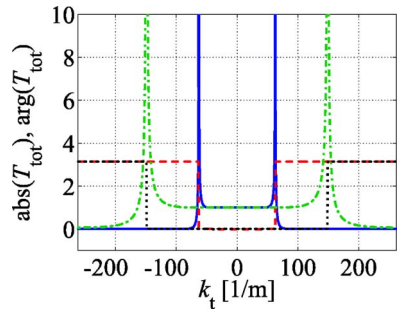

FIG. 11. (Color online) Total transmission from the source plane to the image plane as a function of k_t. $C=5$ pF, $L=10$ nH, $d=0.012$ m, $\varepsilon_r=2.33$, $Z_{0,\mathrm{TL,BW}}=85\ \Omega$, and $Z_{0,\mathrm{TL,FW}}=70\ \Omega$. Case 1: $s_1=s_2=0.06$ m, $l=0.12$ m. Case 2: $s_1=s_2=0.024$ m, $l=0.048$ m. Solid line: $|T_{\mathrm{tot}}|$ (case 1), dashed line: $\arg(T_{\mathrm{tot}})$ (case 1), dash-dotted line: $|T_{\mathrm{tot}}|$ (case 2), and dotted line: $\arg(T_{\mathrm{tot}})$ (case 2).

$$\frac{T_{\mathrm{Lens}}}{Z_{0,\mathrm{FW}}}=\frac{Ae^{-jk_{z,\mathrm{BW}}l}-Be^{+jk_{z,\mathrm{BW}}l}}{Z_{0,\mathrm{BW}}}. \tag{41}$$

The resulting equation for the transmission coefficient T_{Lens} is

$$T_{\mathrm{Lens}}(k_t)=\frac{4Z_{0,\mathrm{FW}}Z_{0,\mathrm{BW}}}{(Z_{0,\mathrm{FW}}+Z_{0,\mathrm{BW}})^2e^{+jk_{z,\mathrm{BW}}l}-(Z_{0,\mathrm{FW}}-Z_{0,\mathrm{BW}})^2e^{-jk_{z,\mathrm{BW}}l}}. \tag{42}$$

The total transmission from the source plane to the image plane (see Fig. 10) is then (the distance from the source plane to the lens is s_1, and the distance from the lens to the image plane is s_2)

$$T_{\mathrm{tot}}(k_t)=T_{\mathrm{Lens}}(k_t)e^{-jk_{z,\mathrm{FW}}(s_1+s_2)}. \tag{43}$$

The longitudinal wave number k_z as a function of k_t can be found from the dispersion relations. Let us choose $k_t=k_x$ and $k_y=0$, so that we can plot curves instead of surfaces. T_{tot} as a function of k_t can now be plotted if the frequency is fixed. Let us choose the lengths of the lens system as the following: $l=0.12$ m, $s_1=0.06$ m, and $s_2=0.06$ m. Now we can choose the frequency at which we want to calculate T_{tot}. Let us study the transmission properties at the matching frequency $f=0.7279$ GHz. From (42) and (43) we can plot the magnitude and phase of T_{tot} as a function of k_t, see Fig. 11, case 1. From Fig. 11 it is seen that the lens works quite well for the propagating modes ($-40\ \mathrm{m}^{-1}<k_t<40\ \mathrm{m}^{-1}$), see Fig. 12 for an example of phase restoration in the image plane.

According to Fig. 11, for evanescent modes ($k_t<-41\ \mathrm{m}^{-1}, k_t>41\ \mathrm{m}^{-1}$) the lens works only in a limited range of k_t, where the absolute value of the transmission coefficient T_{tot} is greater than zero. To improve the effect of evanescent waves enhancement, the characteristic impedances should be matched better in the evanescent wave area of k_t. There are several ways to achieve a better matching of the characteristic impedances.

First, there is of course a possibility to change the impedances of the transmission lines, but this is probably not practically realizable because it would require very accurate manufacturing (even a very small deviation from the ideal impedance values destroys the effect of growing evanescent

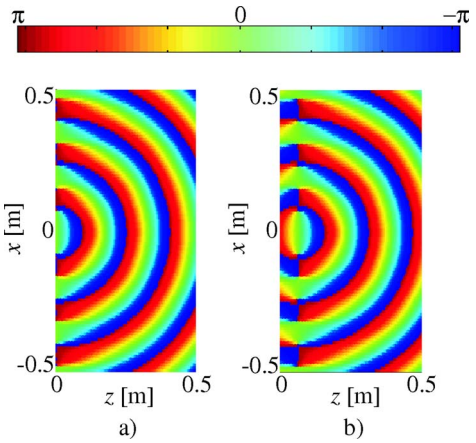

FIG. 12. (Color online) Phase of electric field plotted in a FW network (propagating wave). (a) Source plane is at $z=0$ m. (b) Source plane field multiplied by T_{tot}, back edge of the lens is at $z=0$ m and image plane is therefore at $z=0.06$ m. $C=5$ pF, $L=10$ nH, $d=0.012$ m, $\varepsilon_r=2.33$, $Z_{0,\text{TL,BW}}=85\ \Omega$, and $Z_{0,\text{TL,FW}}=70\ \Omega$. $s_1=s_2=0.06$ m and $l=0.12$ m.

waves). The tuning of $Z_{0,\text{TL,FW}}$ was tested, and using the exact required impedance (see Fig. 9), the transmission of evanescent waves was clearly improved. The resonance peaks in Fig. 11 were moved further away from the center and the absolute value of T_{tot} was larger than or equal to unity approximately for $-100\ \text{m}^{-1}<k_t<100\ \text{m}^{-1}$.

Second, there is a possibility to change the frequency and study if the impedance matching can be made better that way (this also means that the matching of wave numbers k_z is made worse which can also destroy the effect of growing evanescent waves). This was tested, and the best results were obtained using frequency $f=0.729\,05$ GHz. The number of transmitted harmonics was again increased, i.e., the resonance peaks in Fig. 11 were moved further away from the center and the absolute value of T_{tot} was larger than or equal to unity approximately for $-100\ \text{m}^{-1}<k_t<100\ \text{m}^{-1}$.

The third way to enhance the growth of evanescent waves is to change the length of the lens. From (42) it is seen that the growth of evanescent waves is not effective, if the term $(Z_{0,\text{FW}}-Z_{0,\text{BW}})^2e^{-jk_{z,\text{BW}}l}$ in the denominator is large. This term can be made smaller by decreasing the length of the lens l. This is illustrated by Fig. 11, case 2 ($|T_{\text{tot}}|$ is larger than or equal to unity approximately for $-160\ \text{m}^{-1}<k_t<160\ \text{m}^{-1}$) and Fig. 13, where the distances equal $l=0.048$ m, $s_1=0.024$ m, and $s_2=0.024$ m. From Fig. 13 one can conclude that there is a significant growth of evanescent waves in the lens.

By using the shortened lens *and* at the same time tuning the frequency appropriately, it was seen that the transmission coefficient could be made practically ideal (i.e., $|T_{\text{tot}}|=1$ and $\arg(T_{\text{tot}})=0$ for all possible values of k_t). Using the shortened lens and frequency $f=0.7292$ GHz, the absolute values of evanescent fields were indeed almost the same in the image plane and in the source plane (less than 1% difference), see Fig. 13. Notice that in Fig. 13 the dashed line coincides with the solid line in the region $0\ \text{mm}<z<24$ mm and that the field amplitude is not plotted inside the BW region because the transmission coefficient calculated from (43) is used to plot the amplitude values.

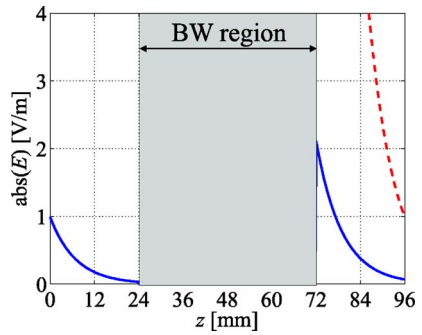

FIG. 13. (Color online) Absolute value of electric field (plots normalized to the value at $z=0$ mm). Solid line: $f=0.7279$ GHz, dashed line: $f=0.7292$ GHz. The source at $z=0$ mm produces only evanescent waves. The source consists of ten harmonics with $k_t=(2\pi n)/(10\times 0.012\ \text{m})$, where $n=-5\cdots 5$. $C=5$ pF, $L=10$ nH, $d=0.012$ m, $\varepsilon_r=2.33$, $Z_{0,\text{TL,BW}}=85\ \Omega$, $Z_{0,\text{TL,FW}}=70\ \Omega$, $s_1=s_2=0.024$ m, and $l=0.048$ m.

VII. SUGGESTIONS FOR A PRACTICALLY REALIZABLE STRUCTURE

A. Proposed structure

How to manufacture the three-dimensional transmission-line networks? The main problem is the ground plane, which should exist in all three dimensions. One solution would be to use coaxial transmission lines (regular in the forward-wave network and loaded with lumped L and C components in the backward-wave network) as shown in Fig. 14(a). This structure is realizable, but we propose a simpler structure based on microstrip lines, as presented in Fig. 14(b). The problem with microstrip lines is of course the design of intersections where the transmission lines from six directions meet. This problem can be overcome by using ground planes which have holes in them at these intersection points. This way the conducting strip can be taken through the substrate and thus connection of the vertical conducting strips becomes possible.

B. Simulation results

The proposed structure [see Fig. 14(b)] has been simulated in ANSOFT HFSS (Version 9.2.1). Due to complexity of the structure and the limited calculation power available, the three-dimensional structure was simulated only near the first lens interface of Fig. 10. The simulated model had $10\times 3\times 3$ $(x\times y\times z)$ unit cells in the forward-wave region and

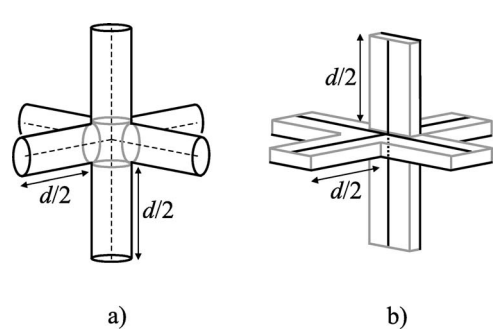

FIG. 14. (a) Unit cell of a 3D forward-wave coaxial network. (b) Unit cell of a 3D forward-wave microstrip network. L and C can be easily implemented as lumped components for both types of backward-wave networks.

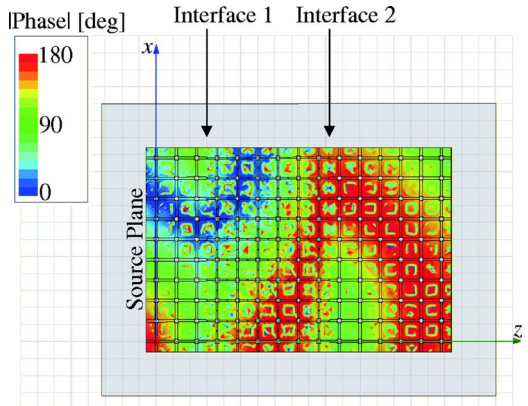

FIG. 15. (Color online) Plot of $|\arg(E_y)|$ in a two-dimensional part of the proposed lens system. The source field is a plane wave with incidence angle $\theta=25°$. The source field is excited at the left edge of the system. $C=5$ pF, $L=10$ nH, $d=0.012$ m, $\varepsilon_r=2.33$, $Z_{0,\mathrm{TL,BW}}=85\ \Omega$, and $Z_{0,\mathrm{TL,FW}}=70\ \Omega$.

$10\times3\times3$ unit cells in the backward-wave region. The properties of the transmission lines and lumped elements were the same as in Fig. 8. The edges of the system were terminated with matched loads to prevent reflections ($R_{\mathrm{BW}}=85\ \Omega$ in the backward-wave region and $R_{\mathrm{FW}}=70\ \Omega$ in the forward-wave region). Different types of source fields (plane waves with different incidence angles and a point source) were tested and in all cases negative refraction was observed at the interface between the forward-wave and backward-wave networks at the expected frequency ($f=0.7279$ GHz).

One layer of the proposed structure, located at $y=0$, was simulated as a complete lens system. Negative refraction was seen at both interfaces, and therefore also focusing of propagating waves was observed. See Fig. 15 for the plot of the phase of the y-directed electric field. The source field is excited at the left edge of the system in Fig. 15. When the field magnitude $|E|$ is plotted and animated as a function of phase, it is clearly seen that the phase propagates to the right in the forward-wave regions and to the left in the backward-wave region. The energy of course propagates to the right in all regions.

VIII. CONCLUSIONS

In this paper we have introduced and studied a three-dimensional transmission-line network which is a circuit analogy of the superlens proposed by Pendry. The structure is a 3D network of interconnected loaded transmission lines. Choosing appropriate loads we realize forward-wave (FW) and backward-wave (BW) regions in the network. The dispersion equations and analytical expressions for the characteristic impedances for waves in FW and BW regions have been derived. Special attention has been given to the problem of impedance and refraction index matching of FW and BW regions. From the derived dispersion equations it has been seen that there exists such a frequency at which the corresponding isofrequency surfaces for FW and BW regions coincide. Theoretically this can provide distortionless focusing of the propagating modes *if* the wave impedances of FW and BW regions are also well matched. Impedance matching becomes even more important when the evanescent modes are taken into account. In this paper we have shown that the wave impedances can be matched at least within 1% accuracy or better if the characteristic impedances of the transmission lines are properly tuned. However, from the practical point of view an accuracy better than 1% is hardly realizable. It has been shown that decreasing the thickness of the BW region reduces the negative effect of the impedance mismatch, while the amplification of the evanescent modes is preserved. We have also outlined a couple of prospective designs of the perfect lens discussed in this paper and numerically simulated performance of one such design.

ACKNOWLEDGMENTS

This work has been done within the frame of the *Metamorphose* Network of Excellence and partially funded by the Academy of Finland and TEKES through the Center-of-Excellence program. The authors would like to thank Dr. Mikhail Lapine for helpful discussions.

[1] J. B. Pendry, Phys. Rev. Lett. **85**, 3966 (2000).
[2] V. G. Veselago, Sov. Phys. Usp. **10**, 509 (1968).
[3] R. A. Shelby, D. R. Smith, and S. Schultz, Science **292**, 77 (2001).
[4] P. Gay-Balmaz and O. J. F. Martin, Appl. Phys. Lett. **81**, 939 (2002).
[5] Th. Koschny, L. Zhang, and C. M. Soukoulis, Phys. Rev. B **71**, 121103(R) (2005).
[6] G. V. Eleftheriades, A. K. Iyer, and P. C. Kremer, IEEE Trans. Microwave Theory Tech. **50**, 2702 (2002).
[7] L. Liu, C. Caloz, C.-C. Chang, and T. Itoh, J. Appl. Phys. **92**, 5560 (2002).
[8] A. Sanada, C. Caloz, and T. Itoh, IEEE Trans. Microwave Theory Tech. **52**, 1252 (2004).
[9] A. Grbic and G. V. Eleftheriades, IEEE Trans. Antennas Propag. **51**, 2604 (2003).
[10] A. Grbic and G. V. Eleftheriades, IEEE Trans. Microwave Theory Tech. **51**, 2297 (2003).
[11] A. Grbic and G. V. Eleftheriades, Phys. Rev. Lett. **92**, 117403 (2004).
[12] A. Grbic and G. V. Eleftheriades, J. Appl. Phys. **98**, 043106 (2005).
[13] G. Kron, Phys. Rev. **64**, 126 (1943).